Asian Journal of Pharmaceutical Sciences 17 (2022) 630–640

Available online at www.sciencedirect.com

ScienceDirect

journal homepage: www.elsevier.com/locate/AJPS

Original Research Paper

Small extracellular vesicles encapsulating lefty1 mRNA inhibit hepatic fibrosis

*Yarong Zhao, Yang Yu, Simiao Wang, Jiaxin Li, Lesheng Teng**

School of Life Sciences, Jilin University, Changchun 130012, China

ARTICLE INFO

Article history:
Received 10 May 2022
Revised 4 July 2022
Accepted 24 July 2022
Available online 18 August 2022

Keywords:
Liver fibrosis
Hepatic stellate cells
Small extracellular vesicles
Transforming growth factor β1
Lefty1

ABSTRACT

Liver fibrosis is the deposition of extracellular matrix (ECM) in the liver caused by persistent chronic injury, which can lead to more serious diseases such as cirrhosis or cancer. Blocking the effect of transforming growth factor β1 (TGF-β1), one of the most important cytokines in liver fibrosis, may be one of the effective ways to inhibit liver fibrosis. As a kind of natural nano-scale vesicles, small extracellular vesicles (sEvs) have displayed excellent delivery vehicle properties. Herein, we prepared hepatic stellate cell (HSC)-derived sEvs loading left-right determination factor 1 (lefty1) mRNA (sEvLs) and we wanted to verify whether they can inhibit fibrosis by blocking the TGF-β1 signaling pathway. The results showed that sEvLs had effective cell uptake and reduced activation of HSCs. Rats that were injected with CCl_4 by intraperitoneal injection for 6 weeks exhibited obvious symptoms of liver fibrosis and were treated with systemically administered sEvLs and free sEvs for 4 weeks. Rats injected with olive oil alone served as sham controls. Administration of sEvLs significantly reduced the area of fibrosis compared with free sEvs. We demonstrated that sEvLs inhibited HSCs activation and ECM production, and promote ECM degradation by downregulating α-smooth muscle actin (α-SMA), collagen I, tissue inhibitor of metalloproteinase (TIMP) -1 and upregulating matrix metalloprotease (MMP) -1. In summary, as an endogenous delivery vehicle, sEvs could deliver mRNA to attenuate hepatic fibrosis by blocking the TGF-β/Smad signaling pathway.

1. Introduction

Liver fibrosis is a pathological feature of wound healing following persistent liver injury, which shows the liver exhibits fibrous scarring with excessive deposition of extracellular matrix (ECM) [1,2]. Liver fibrosis is mostly transformed from chronic liver diseases such as viral hepatitis, alcoholic steatohepatitis (ASH), and non-alcoholic steatohepatitis (NASH) [3,4] and will gradually progress to cirrhosis and liver cancer without prompt treatment.. Therefore, timely prevention of liver fibrosis can improve the severe situation of chronic liver disease with high incidence. The ECM is mainly secreted by myofibroblasts,

* Corresponding author.
E-mail address: tenglesheng@jlu.edu.cn (L. Teng).
Peer review under responsibility of Shenyang Pharmaceutical University.

https://doi.org/10.1016/j.ajps.2022.07.004

which are activated and differentiated from hepatic stellate cells (HSCs) [5,6]. Following liver injury, quiescent HSCs residing in the hepatic sinusoid space of Disse are activated, transdifferentiate into myofibroblasts and secrete α-smooth muscle actin (α-SMA) and other ECM proteins such as collagen and fibronectin [7–9]. During initial injury, they are involved in tissue repair, while they over-repair the injury and out of balance during chronic injury, ultimately resulting in fibrotic collagen deposition.

Transforming growth factor β (TGF-β) 1 is a member of the TGF-β superfamily and is the most widely studied isoform in liver fibrosis, which is considered to be one of the major pro-fibrotic cytokines in the activation of HSCs [10]. TGF-β1 is either autocrine from activated HSCs or paracrine from other cells to further stimulate the activation of HSCs in the injured liver, depending on canonical and non-canonical pathways [11]. The inactive TGF-β1 becomes active after it binds to latency-associated protein (LAP) and is cleaved by specific proteases [12]. Active TGF-β1 binds to TGF type II receptors(TGF-βRII) on the cell membrane surface to promote the tetramerization and phosphorylation of the tetrameric receptor complex composed of TGF-β receptors I (TGF-βRI) and TGF-βRII, followed by phosphorylation of Smad2/Smad3 triggers a signaling cascade which initiates a classical Smad-dependent signaling pathway [13–15]. Furthermore, TGF-β1 activates non-canonical pathways, such as mitogen-activated protein kinase (MAPK), mammalian target of rapamycin (mTOR), PI3K/Akt, JAK1/STAT3, etc., and also promotes HSCs activation [16]. Downstream proteins of the TGF-β1 signaling pathway, including α-SMA, collagen, and tissue inhibitor of matrix metalloproteinase (TIMP), were significantly increased, while matrix metalloproteinase (MMP) expression was inhibited, leading to excessive deposition of ECM and fibrosis [12,17]. Subsequently, studies have found that left-right determination factor (lefty) 1, as a member of the TGF superfamily, inhibits Smad2/3 phosphorylation and collagen synthesis driven by TGF-β1 and it is expected to act as inhibitors of TGF-β family members [18,19]. Lefty1 and lefty2 had been observed in mice and studied in vertebrate left-right asymmetry, regulating left-right patterning by antagonizing nodal activity during embryonic development earlier [20–22]. When studies shifted the perspective to the relationship between homeostasis of ECM and TGF-β1, they found that abnormal overexpression of TGF-β1 leads to tissue fibrosis, while lefty negatively regulates the transcription and expression of collagen, reducing ECM deposition [19,23]. Lefty may lead to TGF-β signaling pathway repression by disrupting Smad2/3 phosphorylation, heterodimerization, Smad4 phosphorylation or formation of R-Smad/Smad4 complexes [24]. And the role of lefty1 in antagonizing TGF-β1 has been demonstrated in a variety of diseases, including fibrotic nephropathy [19], myocardial infarction-induced cardiac fibrosis [25]. These findings suggested that lefty1 significantly inhibited the activation of the TGF-β1/Smad pathway, reduced epithelial-mesenchymal transition (EMT) and ECM synthesis in model mice, and alleviated the symptoms of fibrosis.

Lefty1 may mediate the blockade of TGF-β1 signaling pathway to inhibit the activation of HSCs. However, HSCs exist in the gap between hepatic sinusoidal endothelial cells (HSECs) and hepatocytes, where excessive ECM deposition hinders the delivery of anti-fibrotic drugs [26]. Finding an effective delivery vehicle is extremely important for the treatment of liver fibrosis. Small extracellular vesicles(sEVs) are nanovesicles secreted by cells, including exosomes, microvesicles and apoptotic bodies, which are important mediators of intercellular communication delivering proteins, nucleic acids and lipids [27–29]. As a natural nanoscale extracellular vesicle, sEVs have unique delivery advantages, such as a natural homing ability to source cells and intercellular transfer function for biomolecules [30,31]. Similar structure to cell membranes allows them to have more dominant cellular uptake [32]. Compared with other non-biological drug delivery vehicles, sEVs have excellent biocompatibility, limited immunogenicity and low toxicity [33–35].

There have been many studies on the development of sEVs as a new type of drug system, but there are few studies on the treatment of liver fibrosis. Here, we prepared SEVs containing lefty1 mRNA (sEvLs) and drug-free sEVs (sEvs) from HSC-T6. These sEvLs are used as therapeutic agents in anti-fibrosis studies *in vitro* and *in vivo*. We hypothesized that such sEvLs that deliver mRNA can be more conducive to the uptake of activated HSCs and much more accumulate in HSCs, instead of being blocked by ECM. The results *in vitro* and *in vivo* confirmed our hypothesis. Currently, the treatment of liver fibrosis lacks systematic treatment methods. Small extracellular vesicles, as a potential drug delivery platform, can better break through the ECM and deliver nucleic acid drugs to activated HSCs for functional delivery. It provides an alternative therapeutic direction for the treatment of liver fibrosis and makes a certain contribution to the prevention of liver cirrhosis and even cancer.

2. Materials and methods

2.1. *Materials*

DMEM and penicillin-streptomycin-glutamine (100×) were purchased from Gibco (Waltham, MA, USA). Fetal bovine serum (FBS) was purchased from Procell Life Science & Technology Co.,Ltd (Wuhan, China). Exosome-depleted FBS was purchased from Cellmax Cell Technology Co., Ltd. (Beijing, China). Lefty1 recombinant plasmid (Gene ID: 498299), negative plasmid and GAPDH primers, U6 primers, α-SMA primers, lefty1 primers were purchased from Genepharma Technology Co., Ltd (Shanghai, China). PKH26 was got from Sigma (St. Louis, MO, USA). TransExo^{TM} serum/plasma exosome total RNA extraction kit and PrimeScript RT master mix were got from TransGen Biotech Co., Ltd (Beijing, China). Plasmocin^{TM} prophylactic, dextran-AlexaFluor555, transferrin-AlexaFluor 555, cholera toxin subunit B-AlexaFluor 555 and DiR were purchased from Invivogen (San Diego, CA, USA). Hoechst33342 and lysotracker green were purchased from Beyotime Biotechnology Co., Ltd. (Shanghai, China). Anti-CD9(ab92726), CD81(ab109201), TSG101 (ab125011), α-SMA(ab7817), collagen I(ab270993) and HRP coupling goat anti-rabbit IgG (ab205718), goat anti-rabbit IgG H&L (Alexa Fluor 488) (ab150077) were purchased from

Abcam (Cambridge, UK). Anti-alix (T57215) was purchased from Abmart Medical Technology Co., Ltd. (Shanghai, China). Anti-CD63(AF5117), calnexin (AF5362) were purchased from Affinity Biosciences, Inc. (Cincinnati, OH, USA).

2.2. Cell culture

HSC-T6 cells from Cobioer Biotechnology Co., Ltd. (Nanjing, China) were cultured in DMEM with 10% FBS, 1% penicillin-streptomycin and 0.1% plasmocin^{TM} prophylactic at 37 °C, 5% CO_2 incubator (Sanyo Co., Ltd., Japan).

2.3. Electroporation

HSC-T6 cells at a density of 1×10^6 cells/ml were mixed up with 5 μg lefty1 or negative plasmids (Genepharma Co., Ltd., Suzhou, China), separately. The mixture was loaded in a 0.4 cm electroporation cup (Bio-Rad, USA) and operated in the electroporation system (Gene Pulser Xcell, Bio-Rad, USA) at 220 V, 10 ms, 5 pulses, and 0.1 s intervals.

2.4. Extraction and characterization of sEvs

sEvLs and sEvs were prepared by differential centrifugation from a medium in which cells were electroporated with lefty1 plasmid or negative plasmid. Specifically, perform a step-by-step centrifugation procedure at 4 °C. After culturing HSCs for 24 h, the cell culture medium was centrifuged at 300 g for 10 min to remove cells, 2000 g for 10 min to remove cell debris and apoptotic bodies, and 10 000 g for 20 min to remove large microvesicles. Medium supernatant was then filtered through a sterile 0.22 μm filter to remove vesicles larger than 220 nm. Finally, the pellet was collected by ultracentrifugation twice at 100 000 g for 70 min each. sEvs were assessed by protein quality measured by the BCA protein detection kit (Thermo Fisher Scientific, Waltham, MA, USA).

The morphology of sEvLs and sEvs was observed by a transmission electron microscope (TEM). Diluted sEvLs and sEvs (10 μl) were dropped on the copper grids (300 mesh) covered with a carbon support film and kept for 2 min to remove the excess droplets. 2% uranyl acetate dihydrate was used for staining. sEvLs and sEvs were observed in the JEM-2100F 200 kV (Japan Electronics Corporation, Japan).

The particle size and concentration of sEvLs and sEvs were detected by qNano Gold (Izon, New Zealand). Follow the instructions step by step to detect the particle size and concentration of sEvLs and sEvs suspended in measurement electrolyte with NP150 nanopore. Calibration sample was CPC100 (particle size is 100 nm and concentration is $1.4\,E+13$ particles/ml).

Malvern ZS90(Malvern Panalytical Ltd, UK) was used to detect the zeta potential of sEvLs and sEvs.

The enriched proteins in sEvLs and sEvs were compared with the intracellular proteins to verify the sEvs. Cellular or sEvs' protein (10 μg) was analyzed by western blot. Anti-CD9, CD81, TSG101, Alix, calnexin were diluted 1000-fold and incubated with the protein on the PVDF membrane overnight at 4 °C. HRP coupling goat anti-rabbit IgG (1: 2000) was used to bind to the primary antibody for 4 h. Finally, proteins of different molecular weights were visualized by enhanced chemiluminescence solution combined with HRP, and the bands were photographed under the cooling CCD camera of the imaging system.

To analyze mRNA levels, the TransExo^{TM} serum/plasma exosome total RNA extraction kit was used to extract RNA from sEvLs and sEvs. RNA from HSC-T6 also extracted. The primers for rat lefty1 are as follows: forward, TGGATCCTAGAACCCCCAGG; reverse, CCCAGAAATGGCCACCTGAT. The rat GAPDH primers are as follows: forward, ATGTTCCAGTATGACTCTA; reverse, CACCCCATTTGATGTTAG. U6 primers are as follows: forward, ATGTTCCAGTATGACTCTA; reverse, ATGTTCCAGTATGACTCTA. Real-time fluorescent quantitative PCR was performed to determine the content of lefty1 mRNA in sEvs or cells relative to U6 or GAPDH. RT-qPCR was carried out in CFX96TM Real-Time System (Bio-Rad, USA) and the amplification parameters were 94.0 °C for 5 s, 55.0 °C for 15 s, 72.0 °C for 30 s, 40 cycles. Set the melting curve to determine the amplification efficiency. All RT-qPCR reactions were repeated three times, and the $2^{-\Delta\Delta Ct}$ method was used to calculate the mRNA expression relative to GAPDH.

2.5. sEvs staining

Disperse PKH26 or DiR (1 μl, 1 mM) and sEvs or sEvLs (10 μg) in 500 μl Diluent C respectively, then mix dye and sEvs or sEvLs to incubate for 15 min at room temperature. Extra dye is removed by centrifugation at 100 000 g for 70 min. Dye-labeled sEvs or sEvLs were redispersed in PBS and stored at 4 °C in the dark for a short time.

2.6. Cell uptake

HSC-T6 was pre-treated with recombinant TGF-β1 (10 nM) for 24 h to activate. PKH26 labeled sEvLs (10 μg per well) were incubated with activated HSC-T6 (1×10^5 cell per well) for 1 h, 2 h, and 4 h. After removing the medium, the cells washed with pre-chilled PBS were collected. Finally, the cells fixed with 4% paraformaldehyde were analyzed for their fluorescence intensity using Cytoflex(Beckman, USA). Only the activated cells were used as control. Each experimental group was repeated 3 times, and finally, the average fluorescence intensity of the cells was used as the sEvLs uptake for data statistics.

2.7. Internalization

The cells were seeded on cell slides at a density of 2×10^5/ml and cultured for 24 h. The cells were treated with sEvLs labeled with PKH26 for 0.5 h, 1 h, 2 h. After removing the medium and washing, lysotracker green (0.2 μM) and HSC-T6 were incubated at 37 °C for 30 min. After washing twice with PBS, cells were treated with anti-fluorescence quenching solution containing Hoechst 33,342 nuclear dye. Finally, observe the co-localization of cells and sEvLs under a laser confocal microscope (LSM710, Carl Zeiss, Germany).

HSC-T6 inoculated on the slide was treated with transferrin (0.1 mg/ml), dextran (1 mg/ml) and cholera toxin subunit B (0.005 mg/ml) labeled with Alexa Fluor 555 at 37 °C for 1 h. After the medium was removed, DiR-labeled sEvLs

(10 μg per well) were added for 2 h. Finally, the fixed cells were treated with an anti-fluorescence quenching solution containing Hoechst 33,342 nuclear dye. Observe the path of being taken up of sEvLs and sEvs under a laser confocal microscope. In order to further prove the mechanism of endocytosis, three internalization inhibitors acted on activated HSC-T6 before the uptake of PKH26-labeled sEvLs. Sucrose (0.4 M) was used to inhibit clathrin, cytochalasin (5 μM) was used to inhibit the giant pinocytosis pathway of sugar transport, and nystatin (50 μM) was used to inhibit lipid rafts. Flow cytometry was used to detect the HSC-T6 uptake of sEvLs under different inhibition to illustrate the pathway of sEvs into the cell.

2.8. *Cellular immunofluorescence*

The cells activated by TGF-β1 (10 nM) were treated with sEvLs and sEvs for 48 h, and then the medium was removed. Cells were fixed with 4% paraformaldehyde then and permeabilized with 0.3% TritonX-100 (in PBS) for 20 min at room temperature. The different groups were treated with α-SMA antibody (1:200) to incubate overnight at 4 °C, and then washed 5 times with PBS, each for 5 min. After incubating the cells with AF488-labeled secondary antibody (1:500) for 2 h, they were washed 5 times with PBS for 5 min each time. The cells were treated with anti-fluorescence quenching solutions containing Hoechst 33,342 nuclear dye, and finally, the expression of α-SMA in the cells was observed under a laser confocal microscope and quantification with Image J. Inactivated HSC-T6 was a negative control.

2.9. *Down-regulation of ECM proteins*

Activated or not active HSC-T6 cells were treated with sEvLs and sEvs for 48 h, and then they were cleaved to extract the protein and semi-quantitative by western blot. The changes of lefty1, collagen I, TIMP-1 and MMP-1 had been detected in all. The contents were semiquantitative with Image J.

2.10. *Liver fibrosis rats*

Wistar rats, male, were bred adaptively for 1 week under SPF feeding conditions to ensure free drinking and eating. All animal experiments have been approved by the Experimental Animal Welfare Ethics Committee of Jilin University. (SY202009015). Rats were intraperitoneally injected twice a week with a mixture of CCl_4 and olive oil (1:1, V/V, 1 ml/kg) for 4 to 6 weeks. At the same time, sham operation rats were injected with olive oil (1 ml/kg) as a control. Observe and record the rat's vital signs, diet, activity, and coat gloss every week, and measure the rat's body weight every three days.

From the 4th week to the 6th week, 3 rats from the model group and sham group were sacrificed to take out the liver tissues. After making paraffin sections, the degree of fibrosis of the rat liver was evaluated by H&E and Masson staining.

2.11. *Organization distribution*

The successfully modeled hepatic fibrosis rats were randomly divided into 2 groups, 3 rats in each group, and sEvLs (300 μg/ml/kg) labeled with PKH26 dye were injected into the tail veins. The rats were sacrificed 4 h later and the heart, liver, spleen, lung, and kidney were taken out for imaging to detect the distribution of sEvLs in different tissues. In order to further compare the distribution of sEvLs in liver tissues, frozen sections of the liver were labeled with anti-α-SMA and AF488-labeled secondary antibodies for activated HSCs and DAPI for nucleiar. The fluorescence distribution of liver sections was photographed under a confocal microscope.

2.12. *Anti-fibrosis in vivo*

After modeling successfully, the rats in the model or sham operation group with similar body weight and good growth state were randomly divided into 4 groups with 6 rats in each group. Rats in the sham-operated group were injected with saline. The rats in the model group were intravenously injected with saline, sEvs and sEvLs (150 μg/ml/kg), twice a week, and the body weight of the rats was recorded (data

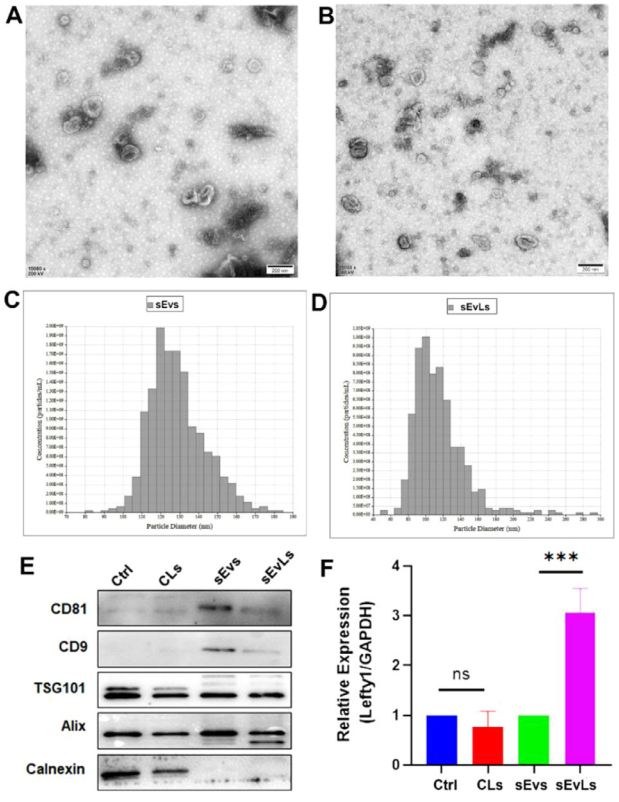

Fig. 1 – Characterization of sEvs and sEvLs. (A, B) Morphologies of sEvs and sEvLs obtained by 200 kV TEM on a scale of 200 nm. (C, D) Particle size of sEvs and sEvLs detected by Qnano gold in electrolysis buffer (E) Western blot detection of the proteins of HSC-T6 (Ctrl), HSC-T6 transfected with lefty1 (CLs), sEvs and sEvLs: CD81, CD9, TSG101, Alix and calnexin. (F) RT-qPCR detection of relative levels of lefty1 mRNA in cells and vesicles to characterize the loading rate of lefty1 mRNA in Ctrl, CLs, sEvs and sEvLs. Data were presented as means and error bars, and t-tests were used to compare significance between two groups. ns: $P>0.5$;*:$P<0.001$.**

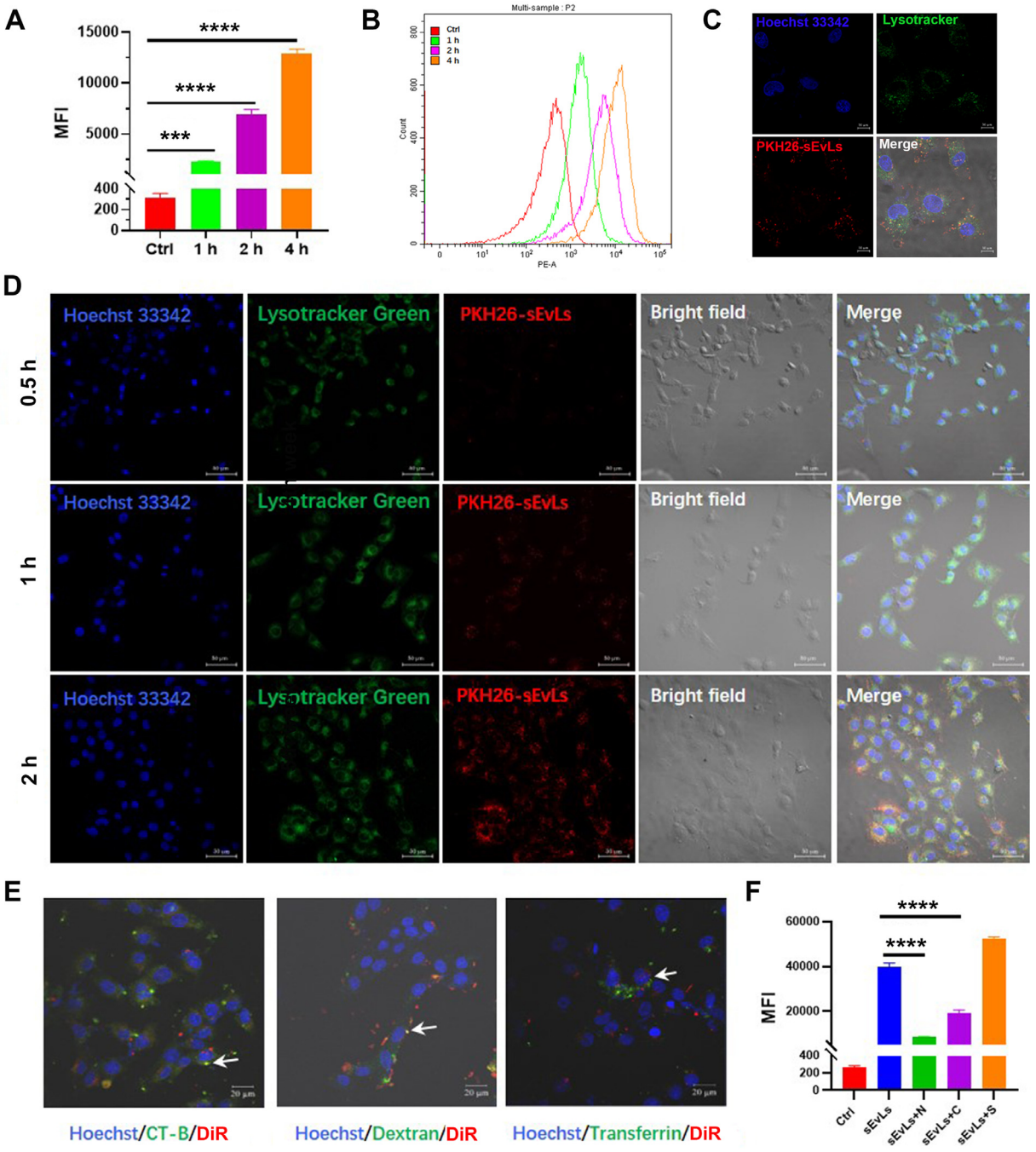

Fig. 2 – Internalization of sEvLs by activated HSC-T6. Mean fluorescence intensity (A) and fluorescence shift curves (B) of activated HSC-T6 after uptake of sEvLs for 1 h, 2 h, and 4 h. (C) Image captured by a 63x oil lens with a confocal laser after 2 h incubation of sEvLs and HSC-T6. Blue is nuclei labeled with Hoechst33342, green is acidic endosomes with Lysotracker Green (0.2 nM), red is PKH26 (1 μM) labeled sEvLs (10 μg/ml). Scale is 10 μm. (D) Colocalization of HSC-T6 and sEvLs after incubation for 0.5 h, 1 h, and 2 h, respectively, on a scale of 50 μm. (E) Co-localization of sEvLs labeled with DiR (1 μM) and HSC-T6 after fluorescent labeling of different endocytic pathways. Labeled with dextran-Alexa Fluor 555 (1 mg/ml), transferrin-Alexa Fluor 555 (0.1 mg/ml), and cholera toxin subunit B -Alexa Fluor 555 (5 μg/ml) are shown in green in the figure. Scale is 20 μm. (F) Comparison of mean fluorescence intensity of cells ingesting PKH26-labeled sEvLs following nystatin (50 μM) (sEvLs+N), cytochalasin B (5 μM) (sEvLs+C), and sucrose (0.4 M) (sEvLs+S) inhibitors. Data were presented as means and error bars, and one-way ANOVA were used to compare significance between groups.*:P>0.001; ****:P<0.0001.**

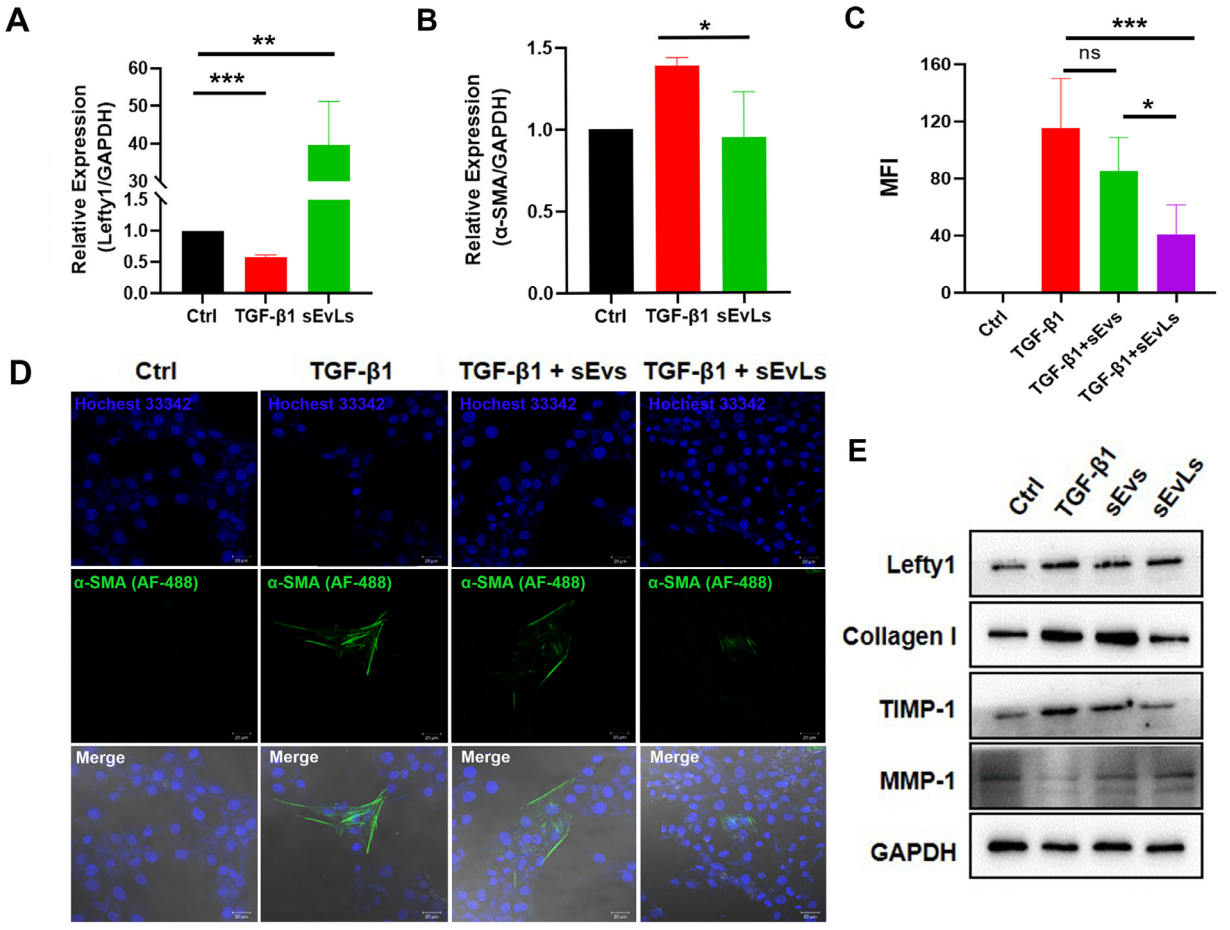

Fig. 3 – Inhibition of the activated HSCs and down-regulation ECM by sEvLs. The effect of sEvLs (10 μg/ml) on the transcription of lefty1 (A) and α-SMA (B) in HSC-T6 was compared with inactivated and activated HST-T6 (10 nM TGF-β1 treated HSC-T6 for 24 h). Each group had 3 repeats, using 2^ (-ΔΔCt) value is used to calculate the transcription level of lefty1 relative to the GAPDH. (C, D) ImageJ for semi-quantification of mean fluorescence intensity in the green channel of α-SMA after 48 h of HSC-T6 activated by 10 nM TGF-β1 treated with sEvLs (10 μg/ml). Scale is 20 μm. (E) After TGF-β1 (10 nM) activated HSC-T6, the protein electrophoresis bands of lefty1, collagen I, TIMP-1, MMP-1 and GAPDH in different treatment groups. Data were presented as means and error bars, and one-way ANOVA was used to compare significance between two groups. ns:P>0.05; *:P<0.05; **:P<0.01; ***:P<0.001.

not shown). Three days after the last administration, the rats were anesthetized and blood and organs were taken for testing. H&E, Masson, Sirus red were performed on the liver tissue to compare the liver histopathology and collagen fiber content between different groups. The level of hydroxyproline in the liver tissue is used to evaluate collagen content. Elisa kit detected the concentrations of TGF-β1 in liver tissue. The liver tissue preserved in the fixative is used for immunohistochemistry to detect the expression of α-SMA.

2.13. *Safety evaluation*

Alanine aminotransferase (ALT) and aspartate aminotransferase (AST) in the tissue of rats are tested to assess liver damage. Heart, spleen, lung, and kidney tissues were made into paraffin sections and stained with H&E to assess tissue damage.

2.14. *Statistics*

The experimental data was carried out in at least 3 replicates and presented as a column chart in the form of mean ± standard deviation (mean ± SD). Comparison of experimental data between groups was carried out with Student's t-test or one-way ANOVA for significance analysis through "GraphPad.Prism.8.0.1.244".

3. Results and discussion

3.1. *Characterization of sEvs and sEvLs*

sEvs and sEvLs were harvested from the culture medium of HSC-T6 electroporated with lefty1 plasmid and blank plasmid. We identified characteristics of sEvs and sEvLs,

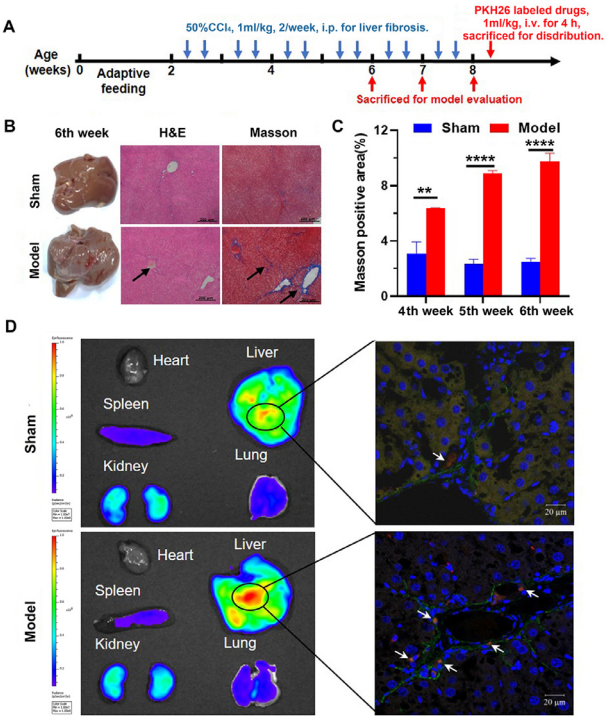

Fig. 4 – Evaluation of the fibrosis rat model induced by CCl_4 and distribution of sEvLs *in vivo*. (A) Model establishment timeline. (B) At 6th week after intraperitoneal injection of 50% CCL_4 in rats, liver tissues were harvested and made into paraffin sections for H&E and Masson staining. The model group was compared with the sham operation group injected with olive oil. (C) Masson staining fibrosis positive area calculated by Image J is quantified. (D) PKH26 labeled sEvLs (300 μg/ml/kg) were injected into sham and model rats via the tail vein and observed the fluorescence distribution in different tissues 4 h after injection. Co-localization of sEvLs and α-SMA in liver tissue sections (blue is DAPI, labeled nucleus; green is a fluorescent secondary antibody labeled with Alexa Fluor 488, red is sEvLs labeled with PKH26). Data were presented as means and error bars, and t-tests were used to compared significance of two groups. **:P<0.01;**:P<0.0001.**

that included morphological observation, particle size, zeta potential, concentration and special membrane protein. These results were shown in Fig. 1 and Fig. S1. Fig. 1A and 1B showed the morphologies of sEvs and sEvLs respectively, which were vesicles with a depression in the middle after dehydration, and the size of the vesicles seemed to be no more than 200 nm visibly. Fig. 1C showed the particle size and concentration of sEvs, with an average particle size of 129 ± 14.6 nm and a concentration of 1.06 $E+9$ particles/ml. The average particle size of sEvLs was 113 ± 19.6 nm and the concentration was 9.91 $E+9$ particles/ml (Fig. 1D), which was similar to the particle size and concentration of sEvs. It was found that there was a certain relationship between membrane protein concentration and particle concentration. When the membrane protein concentration was 1 mg/ml, the particle concentration was determined to be 10^{11} particles/ml, which provided a reference for the dosage of sEVs in subsequent cell and animal experiments. Results of zeta potential showed that both sEvs and sEvLs had negative potentials, respectively −6.14 mV and −13.4 mV (Fig. S1). For enriched proteins in vesicles, such as CD81, CD9 of the tetraspanin family [36], ESCRT complex component proteins TSG101, Alix [37] were all detected in sEvs and sEvLs, while the endoplasmic reticulum protein calnexin was found only in cell lysates (Fig. 1E). Pre-loading of therapeutic nucleic acids in sEVs was based on the fact that mRNAs were detected in exosomes, it is suggested that mRNA could be actively packaged into sEVs which in turn transfected donor cells with coding DNA to indirectly load nucleic acid and obtain drug-loaded sEVs. The relative content of lefty1 mRNA in cells and vesicles showed that the lefty1 mRNA in sEvLs was 2-fold higher than that in sEvs, likely due to loading of the plasmid-encoded lefty1 mRNA, which successfully confirmed the pre-loading of therapeutic nucleic acids in sEvLs (Fig. 1F). The loading efficiency of this method depends on the transfection efficiency of the plasmid and the sorting mechanism of mRNA into sEVs, so that is not controllable.

3.2. *Internalization of sEvLs*

To demonstrate that the modified sEvLs can be taken up by activated HSCs, we co-incubated TGF-β1-treated HSCs with PKH26-labeled sEvLs for 1, 2 and 4 h, respectively. The fluorescence intensity in cells was detected by flow cytometry to indicate the uptake ability of cells to sEvLs. The results were shown in Fig. 2A and 2B. With the prolongation of co-incubation time, the mean fluorescence intensity in HSC-T6 increased significantly. Confocal laser microscopy also was used to observe uptake changes in sEvLs entering cells from a small amount of cellular internalization at 0.5 h to more co-localization of sEvLs and acidic endosomes at 2 h. (Fig. 2C and 2D).

After dextran – Alexafluor555 (1 mg/ml), transferrin - AlexaFluor555 (0.1 mg/ml), cholera toxin subunit B – AlexaFluor555 Conjugate (5 μg/ml) marked macropinocytosis, clathrin and lipid raft-mediated endocytosis separately, or inhibiting these pathways by cytochalasin B (5 μM), sucrose (0.4 M), nystatin (50 μm), we explored internalization mechanism of DiR-labeled or PKH26-labeled sEvLs by HSC-T6. The results showed that sEvLs may enter HSC-T6 more through cholera toxin subunit B and dextran-tagged lipid rafts and macropinocytosis pathways than clathrin(Fig. 2E and 2F). The results observed by confocal were consistent with the results of flow cytometry, compared with HSC-T6 without any endocytosis inhibitor. HSC-T6 after sucrose treatment uptake more sEvLs, while the uptake of nystatin and cytochalasin B treatment was extremely significantly reduced, especially nystatin (Fig. 2E). Cells had been shown to take up sEVs through multiple endocytic pathways, including clathrin-dependent endocytosis, caveolin-mediated uptake, macropinocytosis, phagocytosis, and lipid raft-mediated internalization [38]. Due to the heterogeneity of extracellular vesicles and differences in source cells, our results showed that sEvLs derived from HSC-T6 may be taken up by activated HSCs mainly through macropinocytosis and lipid raft-mediated endocytic pathways.

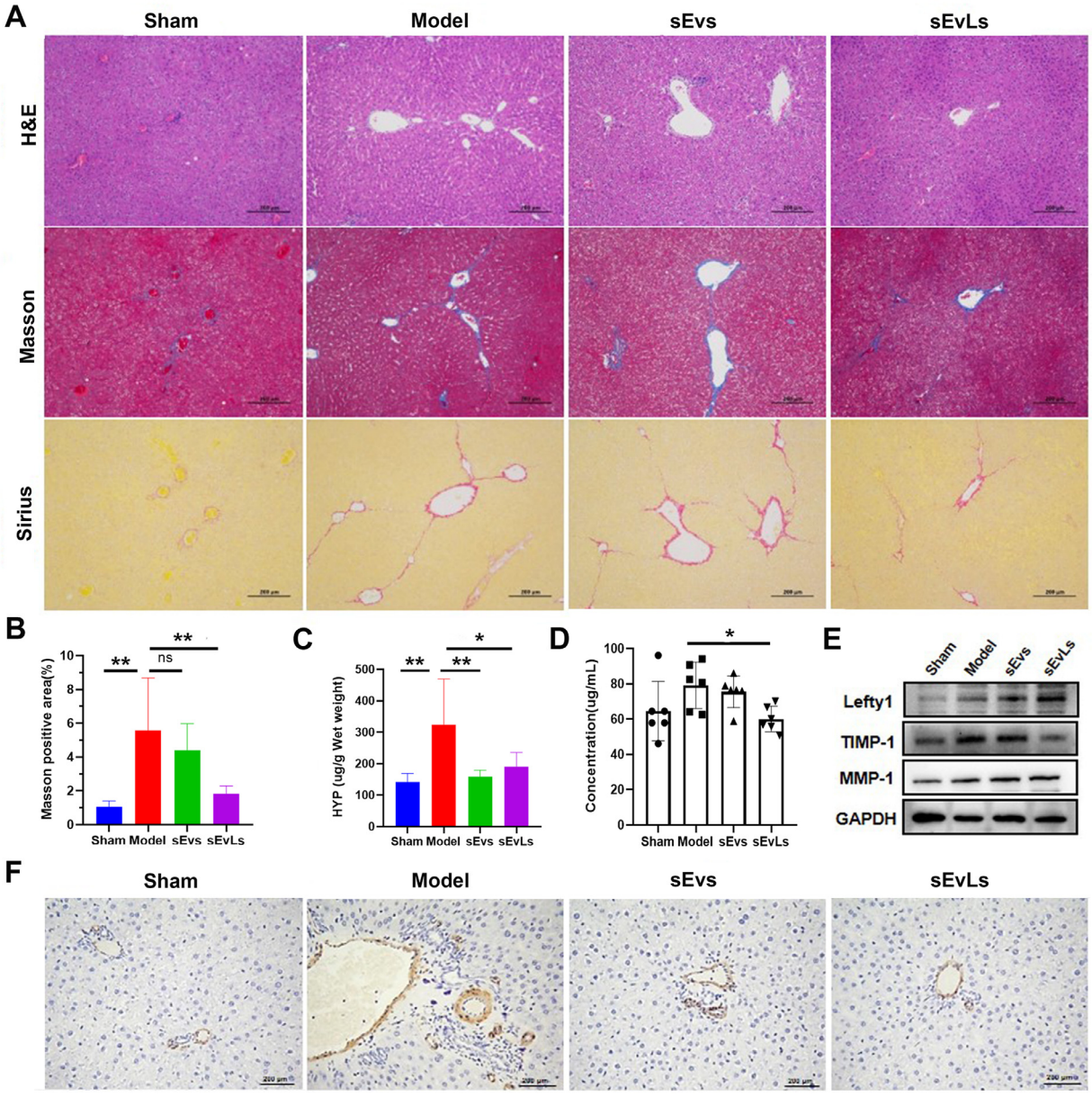

Fig. 5 – Anti-fibrotic evaluation of sEvLs *in vivo*. (A) H&E, Masson and Sirius stained liver tissue in the sham and the model group after injection of saline, sEvs and sEvLs. Scale is 200 μm. (B) Masson staining fibrosis positive area calculated by Image J in different groups. (C) Hydroxyproline in liver tissues of different groups. (D) Concentrations of TGF-β1 in liver tissue after treatment in different groups. (E) Western blotting was used to detect the expression of lefty1, TIMP-1, MMP-1, and GAPDH in liver tissues in different groups. (F) Immunohistochemistry was used to detect the expression of α-SMA in different groups. Data were presented as means and error bars, and one-way ANOVA was used to compared significance between groups. ns:P<0.05; *: P<0.05;: P<0.01.**

3.3. *Inhibition of the activated HSCs and down-regulation ECM*

α-SMA, as a marker for activation of HSCs [39], was used to verify the effect of sEvLs on HSC-T6. After HSC-T6 was treated with different concentrations of TGF-β1 in experiments, according to the transcription of α-SMA mRNA as an indicator of HSC-T6 activation, 10 nM TGF-β1 treatment for 24 h was selected to simulate the activation of HSC-T6 (Fig. S2). Meanwhile, activated HSC-T6 showed lower lefty1 transcription, while sEvLs intake significantly increased its transcription (Fig. 3A). The results showed that α-SMA mRNA was decreased in HSC-T6 after sEvLs treatment (Fig. 3B). Expression of α-SMA in HSC-T6 following only TGF-β1 or simultaneous treatment with TGF-β1 and sEvs and sEvLs was assessed by cellular immunofluorescence (Fig. 3C and 3D). After binding of the Alexafluor488-labeled secondary antibody to α-SMA, we calculated the mean fluorescence intensity in

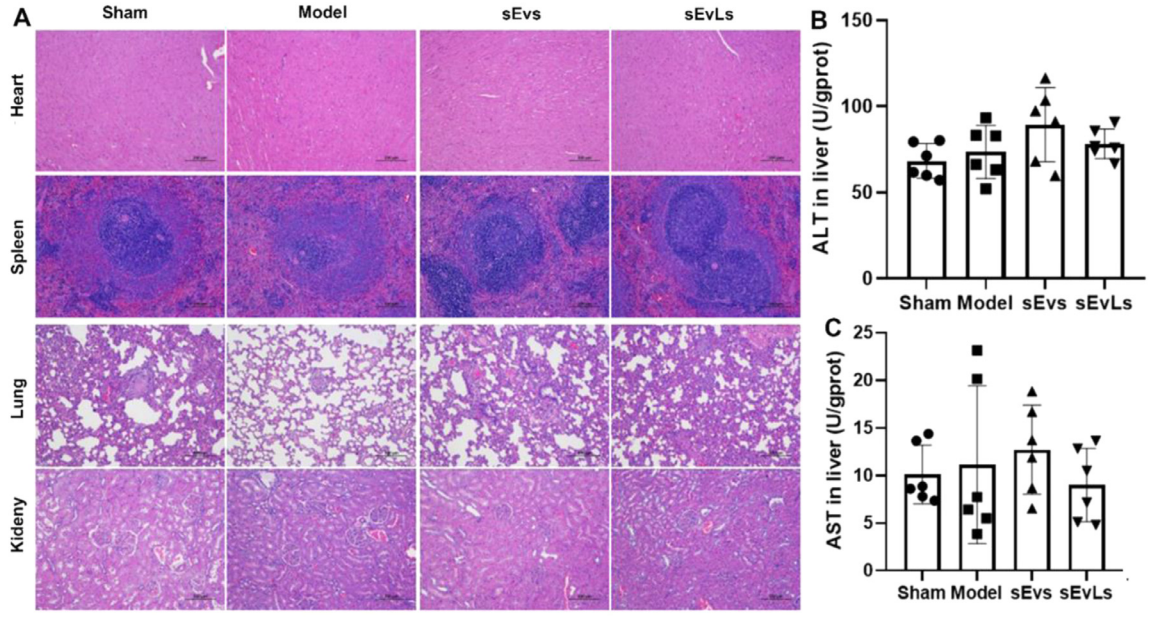

Fig. 6 – Safety evaluation of sEvLs after systemic administration in rats with fibrosis. (A) H&E of heart, spleen, lung and kidney after treatment of rats in sham, model, sEvs and sEvLs group. (B-C) The concentration of ALT and AST in the liver tissues of rats in different groups. Data were presented as means and error bars, and there was no significance between groups by one-way ANOVA.

the green channel using ImageJ. The results showed that the MFI in cells treated with sEvLs was significantly lower than in cells treated with TGF-β1 alone (Fig. 3C), as evident from the confocal photographs (Fig. 3D). This suggested that sEvLs might be able to inhibit the expression of α-SMA in activated HSC-T6 and implied that sEvLs loaded with lefty1 mRNA could inhibit TGF-β1-induced HSC activation.

To further explore the anti-fibrosis, we tested the levels of lefty1, collagen I, TIMP-1 and MMP-1 after treatment of sEvLs and sEvs in activated HSC-T6 (Fig. 3E and Fig. S3). After treatment of HSC-T6 with sEvLs, lefty1 and MMP-1 were up-regulated while both collagen I and TIMP-1 were down-regulated compared to HSC-T6 treated with TGF-β1 alone. Fig.S3 showed the semi-quantitative of lefty1, collagen I, TIMP-1, MMP-1 relative to GAPDH in different treatment groups. Although it was shown that the up-regulation of lefty1 and MMP-1 was not obvious, may be due to the asynchronous expression of lefty1 and MMP-1 with collagen I and TIMP-1 expression in activated HSC-T6. Collagen I is one of the components of the ECM and MMP-1 and TIMP-1 are related to the synthesis and degradation of ECM. The changes in their expression levels indicated that sEvLs may affect the expression of MMP-1, TIMP-1 and collagen I in activated HSC-T6, which is a good news in favor of altering extracellular matrix deposition. This suggested that sEvLs loaded with lefty1 mRNA inhibited TGF-β1-induced HSCs activation and ECM production, and also may promote the degradation of ECM. These results will be further validated in rats.

3.4. *Organization distribution*

Liver fibrosis was induced in rats by intraperitoneal injection of CCl_4 for 6 weeks after adaptive feeding. After 4, 5 and 6 weeks of intraperitoneal injection, H&E and Masson staining were performed on liver tissue to observe inflammatory infiltration and collagen fiber production to evaluate the degree of fibrosis, as shown in Fig. 4B, 4C and Fig. S4. Infiltration of inflammatory cells and generation of collagen fibers (blue) increased over time (Fig. 4B). At the 6th week, the area of collagen fibers reached 9.78%, and most of the portal areas were fibrotic, with a fibrous septum, which was in stage 2 fibrosis according to the Ishak [40]. Fluorescence accumulation in major organs was observed after systemic administration of PKH26-labeled sEvLs in sham-operated and fibrotic rats, showing that most of the sEvLs accumulated in the liver tissue of fibrotic rats, whereas in sham-operated accumulation was less (Fig. 4D). A small part was distributed in the kidney, which may be the cause of kidney metabolism. To further confirm the location of sEvLs in the liver, anti-α-SMA and Alexafluor 488 coupled secondary antibodies were used to detect the co-localization of sEvLs and HSCs. The results showed that sEvLs not only accumulated in the liver but were also taken up by activated HSCs. It implied that sEvLs had the potential to penetrate the ECM, which would overcome a major obstacle in the treatment of liver fibrosis.

3.5. *Inhibition of HSCs activation and ECM production in vivo*

We further examined whether sEvLs delivering lefty1 mRNA could suppress liver fibrosis *in vivo*. The results of Masson staining and Sirius red staining showed that the area of collagen fibers was greatly reduced after sEvLs treatment and that the positive area was reduced to 1.83% (Fig. 5A and 5B).

Likewise, hydroxyproline, a unique amino acid that was one of the main components of collagen, was lower in the liver tissue of sEvLs-treated rats than in the model group (Fig. 5C). These results indicated that sEvLs treatment significantly improved the symptoms of hepatic fibrosis in rats. A significant decrease in tissue concentrations of TGF-β1 was also detected (Fig. 5D). Further discussing the changes in protein levels, we found that compared with the model, the sEvLs-treated group up-regulated lefty1 protein and MMP-1, and down-regulated TIMP-1, which inhibits MMP-1 (Fig. 5E). Their mutual regulation is related to ECM deposition, and this change favors ECM degradation. The IHC results showed that the major protein α-SMA in activated HSCs was also down-regulated (Fig. 5F), implying that the sEvLs treatment group also seemed to inhibit HSCs activation *in vivo*. These results indicated that the sEvLs treatment group alleviated the symptoms of fibrosis, possibly by inhibiting the activation of HSCs mediated by TGF-β1 and promoting the degradation of ECM.

3.6. *Safety assessment*

The histopathological section results of the main organs of liver fibrosis rats showed that the heart, spleen, lung, and kidney had no obvious tissue damage after systemic administration of sEvLs (Fig. 6A). The levels of ALT and AST in the liver of rats showed a decrease after treatment with sEvLs (Fig. 6B and 6C). It proved that the treatment of sEvLs enhanced liver function without causing damage to other tissues, further revealing the safety of the administration of sEvLs, which may be related to their natural origin, without apparent immunogenicity and toxicity.

4. Conclusion

In conclusion, we generated sEVs encapsulating lefty1 mRNA and demonstrated that they contribute to inhibiting TGF-β1-mediated HSC activation and reduce ECM deposition. After systemic administration to rats with CCl_4-induced liver fibrosis, sEvLs were able to penetrate the ECM to accumulate in fibrotic liver tissue and be taken up by activated HSCs. They also show positive anti-fibrotic therapeutic effects. These results suggest that sEVs-based therapies may have great potential as novel anti-fibrotic agents.

Conflicts of interest

The authors report no conflicts of interest.

Acknowledgements

The authors acknowledge the financial support received from National Natural Science Foundation of China (No. 82073784), Jilin Province Science and Technology Development Program (No. 20200801012GH) and Industrial Technology Research and Development Projects from the Development and Reform Commission of Jilin Province (2019C050-4).

Supplementary materials

Supplementary material associated with this article can be found, in the online version, at doi:10.1016/j.ajps.2022.07.004.

REFERENCES

[1] Du Z, Wu T, Liu L, Luo B, Wei C. Extracellular vesicles-derived miR-150-5p secreted by adipose-derived mesenchymal stem cells inhibits CXCL1 expression to attenuate hepatic fibrosis. J Cell Mol Med 2021;25(2):701–15.
[2] Geng W, Li C, Zhan Y, Zhang R, Zheng J. Thymoquinone alleviates liver fibrosis via miR-30a-mediated epithelial-mesenchymal transition. J Cell Physiol 2020;236(5):3629–40.
[3] Chen Z, Jain A, Liu H, Zhao Z, Cheng K. Targeted drug delivery to hepatic stellate cells for the treatment of liver fibrosis. J Pharmacol Exp Ther 2019;370(3):695–702.
[4] Ji Wang Q, Zhao Q, Tong H, Yu M, Wang M, et al. Co-delivery of miR-29b and germacrone based on cyclic RGD-modified nanoparticles for liver fibrosis therapy. J Nanobiotechnology 2020;18(1):86.
[5] Ray K. Liver: hepatic stellate cells hold the key to liver fibrosis. Nat Rev Gastroenterol Hepatol 2014;11(2):74.
[6] Lee C, Kim M, Han J, Yoon M, Jung Y. Mesenchymal stem cells influence activation of hepatic stellate cells, and constitute a promising therapy for liver fibrosis. Biomedicines 2021;9(11).
[7] Sato Y, Murase K, Kato J, Kobune M, Sato T, Kawano Y, et al. Resolution of liver cirrhosis using vitamin A-coupled liposomes to deliver sirna against a collagen-specific chaperone. Nat Biotechnol 2008;26(4):431–42.
[8] Zhang CY, Yuan WG, He P, Lei JH, Wang CX. Liver fibrosis and hepatic stellate cells: etiology, pathological hallmarks and therapeutic targets. World J Gastroenterol 2016;22(48):10512–22.
[9] Wang S, Friedman SL. Hepatic fibrosis: a convergent response to liver injury that is reversible. J Hepatol 2020;73(1):210–211.
[10] Ding N, Yu RT, Subramaniam N, Sherman MH, Wilson C, Rao R, et al. A vitamin D receptor/Smad genomic circuit gates hepatic fibrotic response. Cell 2013;153(3):601–13.
[11] Derynck R, Budi EH. Specificity, versatility, and control of TGF-beta family signaling. Sci Signal 2019;12(570).
[12] Lodyga M, Hinz B. TGF -beta1 - a truly transforming growth factor in fibrosis and immunity. Semin Cell Dev Biol 2020;101:123–39.
[13] Kim BG, Malek E, Choi SH, Ignatz-Hoover JJ, Driscoll JJ. Novel therapies emerging in oncology to target the TGF -beta pathway. J Hematol Oncol 2021;14(1).
[14] Tang LY, Heller M, Meng Z, Yu LR, Tang Y, Zhou M, et al. Transforming growth factor-beta (TGF -beta) directly activates the JAK1-STAT3 axis to induce hepatic fibrosis in coordination with the smad pathway. J Biol Chem 2017;292(10):4302–12.
[15] Hu HH, Chen DQ, Wang YN, Feng YL, Cao G, Vaziri ND, et al. New insights into TGF-beta/Smad signaling in tissue fibrosis. Chem Biol Interact 2018;292:76–83.
[16] Roehlen N, Crouchet E, Baumert TF. Liver fibrosis: mechanistic concepts and therapeutic perspectives. Cells 2020;9(4).
[17] Leask A. Getting to the heart of the matter new insights into cardiac fibrosis. Circ Res 2015;116(7):1269–76.
[18] Fabregat I, Caballero-Diaz D. Transforming growth factor-beta-induced cell plasticity in liver fibrosis and hepatocarcinogenesis. Front Oncol 2018;8:357.

[19] Zhang L, Liu X, Liang J, Wu J, Tan D, Hu W. Lefty-1 inhibits renal epithelial-mesenchymal transition by antagonizing the TGF -beta/Smad signaling pathway. J Mol Histol 2020;51(1):77–87.
[20] Bisgrove BW, Essner JJ, Yost HJ. Regulation of midline development by antagonism of lefty and nodal signaling. Development 1999;126(14):3253–62.
[21] Hamada H, Meno C, Saijoh Y, Adachi H, Yashiro K, Sakuma R, et al. Role of asymmetric signals in left-right patterning in the mouse. Am J Med Genet 2001;101(4):324–7.
[22] Meno C, Shimono A, Saijoh Y, Yashiro K, Mochida K, Ohishi S, et al. Lefty-1 is required for left-right determination as a regulator of lefty-2 and nodal. Cell 1998;94(3):287–97.
[23] Mason JM, Xu HP, Rao SK, Leask A, Barcia M, Shan J, et al. Lefty contributes to the remodeling of extracellular matrix by inhibition of connective tissue growth factor and collagen mrna expression and increased proteolytic activity in a fibrosarcoma model. J Biol Chem 2002;277(1):407–15.
[24] Yang YR, Bu FT, Yang Y, Li H, Huang C, Meng XM, et al. Lefty2 alleviates hepatic stellate cell activation and liver fibrosis by regulating the TGF-beta1/Smad3 pathway. Mol Immunol 2020;126:31–9.
[25] Li CY, Zhang JR, Li XX, Zhao L, Xi H, Hu WN, et al. Lefty1 ameliorates post-infarction fibrosis by suppressing p-Smad2 and p-ERK1/2 signaling pathways. J Cardiovasc Transl Res 2021;14(4):636–46.
[26] Azzam M, El Safy S, Abdelgelil SA, Weiskirchen R, Asimakopoulou A, de Lorenzi F, et al. Targeting activated hepatic stellate cells using collagen-binding chitosan nanoparticles for sirna delivery to fibrotic livers. Pharmaceutics 2020;12(6).
[27] Lim HK, Jeffrey GP, Ramm GA, Soekmadji C. Pathogenesis of viral hepatitis-induced chronic liver disease: role of extracellular vesicles. Front Cell Infect Microbiol 2020;10:587628.
[28] Chiabotto G, Ceccotti E, Tapparo M, Camussi G, Bruno S. Human liver stem cell-derived extracellular vesicles target hepatic stellate cells and attenuate their pro-fibrotic phenotype. Front Cell Dev Biol 2021;9:777462.
[29] Sato K, Kennedy L, Liangpunsakul S, Kusumanchi P, Yang Z, Meng F, et al. Intercellular communication between hepatic cells in liver diseases. Int J Mol Sci 2019;20(9).
[30] Gangadaran P, Ahn BC. Extracellular vesicle- and extracellular vesicle mimetics-based drug delivery systems: new perspectives, challenges, and clinical developments. Pharmaceutics 2020;12(5).
[31] Herrmann IK, Wood MJA, Fuhrmann G. Extracellular vesicles as a next-generation drug delivery platform. Nat Nanotechnol 2021;16(7):748–59.
[32] Ohno S, Drummen GP, Kuroda M. Focus on extracellular vesicles: development of extracellular vesicle-based therapeutic systems. Int J Mol Sci 2016;17(2):172.
[33] Li R, Gong X, Hong C, Wang H, Chen Y, Tan K, et al. An efficient photochemotherapy nanoplatform based on the endogenous biosynthesis of photosensitizer in macrophage-derived extracellular vesicles. Biomaterials 2021;279:121234.
[34] Meng W, He C, Hao Y, Wang L, Li L, Zhu G. Prospects and challenges of extracellular vesicle-based drug delivery system: considering cell source. Drug Deliv 2020;27(1): 585–598.
[35] Tang TT, Wang B, Lv LL, Liu BC. Extracellular vesicle-based nanotherapeutics: emerging frontiers in anti-inflammatory therapy. Theranostics 2020;10(18):8111–29.
[36] Han C, Kang H, Yi J, Kang M, Lee H, Kwon Y, et al. Single-vesicle imaging and co-localization analysis for tetraspanin profiling of individual extracellular vesicles. J Extracell Vesicles 2021;10(3):e12047.
[37] Juan T, Furthauer M. Biogenesis and function of ESCRT-dependent extracellular vesicles. Semin Cell Dev Biol 2018;74:66–77.
[38] Mulcahy LA, Pink RC, Carter DR. Routes and mechanisms of extracellular vesicle uptake. J Extracell Vesicles 2014(3).
[39] Wang Q, Wang LX, Zeng JP, Liu XJ, Liang XM, Zhou YB. Histone demethylase retinoblastoma binding protein 2 regulates the expression of alpha-smooth muscle actin and vimentin in cirrhotic livers. Braz J Med Biol Res 2013;46(9):739–45.
[40] Horani A, Muhanna N, Pappo O, Melhem A, Alvarez CE, Doron S, et al. Beneficial effect of glatiramer acetate (copaxone) on immune modulation of experimental hepatic fibrosis. Am J Physiol Gastrointest Liver Physiol 2007;292(2):G628–38.